CLM-P615

CLM-P615

UKAEA

Preprint

ELECTRON CYCLOTRON RESONANCE HEATING IN SMALL TOKAMAKS

P. J. FIELDING

CULHAM LABORATORY
Abingdon Oxfordshire

1980

CLM-P 615

ELECTRON CYCLOTRON RESONANCE HEATING IN SMALL TOKAMAKS

by

P.J. Fielding

Culham Laboratory, Abingdon, Oxon, OX14 3DB, UK
(Euratom/UKAEA Fusion Association)

Abstract

The application to small, low magnetic field tokamaks of radio frequency heating at the electron cyclotron second harmonic resonance is discussed. For cases where the plasma is optically thin the role of wall reflections is taken into account in a linear calculation of the radial power deposition profiles. Consideration of single-particle motion in the presence of a resonant RF field leads to a simple heuristic analysis of the coupling mechanism and to estimates of the field strengths at which quasi-linear heating phenomena become significant.

(Submitted for publication in Nuclear Fusion)

August 1980

1. INTRODUCTION

1.1 Electron Cyclotron Resonance Heating

The cyclotron resonance interaction between an electron and an electromagnetic wave provides a mechanism for the efficient transfer of energy to a plasma, and has been used for many years in mirror machines [1]. Microwave heating of this type has also been used in levitron confinement devices [2]. In contrast to the moderate demands on source technology to which these applications gave rise, the use of electron cyclotron resonance heating (ECRH) in tokamaks was until quite recently constrained severely by the lack of suitably efficient high-power R.F. sources, capable of operating in the required frequency range. The development of the cyclotron maser concept however has alleviated the source problem to the extent that so-called gyrotron devices are now available [3] which can generate efficiently several hundred kilowatts of R.F. for pulse lengths of the order of ten milliseconds or more, typically at frequencies in the range 20 - 100GHz.

Since the electron Larmor frequency in a magnetic field of 1 tesla is 28GHz, sources of this type are very well suited to ECRH in tokamaks, where the advantage of high source efficiency may be combined with a theoretically high plasma heating efficiency, as is confirmed by experiment [4 - 5]. In addition, source-plasma coupling is possible using standard waveguide techniques which are particularly convenient in minimising problems of access to the torus.

An important feature of ECRH is that the zone of resonance is localised by magnetic field inhomogeneity: electrons in a magnetised plasma can absorb energy from an electromagnetic wave of frequency ω when the condition for cyclotron resonance is fulfilled:

$$\omega - k_{\parallel} v_{\parallel} = n\Omega_B \qquad (1)$$

for some integer n, where $\Omega_B = eB/mc$ is the electron Larmor frequency, $v_\parallel$ and $k_\parallel$ being respectively the component of electron velocity and the component of the wave propagation vector parallel to the magnetic field $\underline{B}$. Within the zone of resonance with thermal electrons ($|v_\parallel| \lesssim V_T$) the magnetic field variation δB is given roughly by $\delta B/B \simeq |k_\parallel| V_T/\omega$, or when $|k_\parallel| \lesssim \frac{V_T}{c}\frac{\omega}{c}$, by $\frac{\delta B}{B} \simeq \left(\frac{V_T}{c}\right)^2$.

The second expression, which represents the minimum resonance zone width for all values of $k_\parallel$, results from the relativistic velocity dependence of the electron mass which is important when the frequency Doppler shift $k_\parallel v_\parallel$ is small [6]. Thus, in tokamaks (and stellarators) where the main inhomogeneity results from the toroidal field, the resonance layer extends vertically within the plasma with a width of order $Rn_\parallel\sqrt{\frac{kT_e}{m_e c^2}}$, or $R\frac{kT_e}{m_e c^2}$ in the relativistic case, where R is the major radius corresponding to resonance, T_e the electron temperature and $n_\parallel = \frac{|k_\parallel| c}{\omega}$. The layer width is generally much less than the radius of plasma cross-section when $n_\parallel$ is small, even at multi-kilovolt temperatures, and in combination with the flux surface geometry this makes possible theoretically the localised heating of electrons at chosen parts of the plasma cross-section, at least when the plasma is optically thick so that absorption in one transit of the layer is complete. For this reason, ECRH may have important future applications to current profile control, in addition to a bulk plasma heating role.

Of the various possible coupling schemes which can be devised, that which is most suitable for large tokamaks makes use of the ordinary (O) mode [7], since typically the plasma is optically thick as desired at the fundamental resonance [7-10], allowing the source

frequency to be as low as possible. In addition this wave may be launched in the appropriate polarisation from an aperture conveniently located on the outside (low magnetic field side) of the torus without encountering any reflective layers in the low density plasma edge.

At sufficiently high electron density n_e, electromagnetic waves will not propagate and the mode cut-off conditions are an important constraint in the use of ECRH. For the ordinary mode cut-off occurs when the electron plasma frequency $\omega_{pe} = \sqrt{\frac{4\pi n_e e^2}{m_e}}$ becomes equal to the wave frequency, and the density limit at fundamental resonance may be expressed in terms of the electron beta

$$\beta_e = \frac{8\pi n k T_e}{B^2} \leq 0.4 T_e \%$$

where T_e is expressed in keV. Although restrictive, this bound is not incompatible with the general requirements for thermonuclear ignition.

1.2 Application to Small Tokamaks

Although future development of ECRH in tokamaks will concentrate on using the O mode, the above argument does not apply to some of the smaller research tokamaks (e.g. TM-3 [4], TOSCA [11], THOR [12]) because under conditions of interest the plasma may be optically thin for this mode, and also because the constraint on source frequency tends to be less important.

However, the plasma in such devices remains optically thick at fundamental resonance to the extraordinary (X) mode even at low temperature due to the process of mode-conversion to Bernstein waves which occurs at the upper hybrid resonance [13]. These slow, quasi-electrostatic modes cannot propagate in vacuo and so remain trapped

within the plasma where cyclotron damping, or at very low temperatures collisional damping [14], can take place. In addition, direct cyclotron damping of the X mode can be effective for oblique angles of incidence. For small tokamaks therefore the X mode can provide an efficient means of coupling R.F. power at fundamental resonance to the plasma electrons, when the O mode damping is weak. It is very inconvenient however that the launching waveguide for the X mode must be mounted on the inside of the torus in order to avoid reflection at the low density cyclotron cut-off [15]. Furthermore, at high temperature the Bernstein wave can be so heavily damped that substantial amounts of power can be absorbed by the small numbers of electrons with large $v_{\parallel}$, before the wave reaches the zone of cyclotron resonance with thermal electrons [14]. This undesirable effect can be minimised by launching waves with small $k_{\parallel}$ [12], however a narrow antenna pattern is then required which in small tokamaks may be difficult to produce. Alternatively, by launching the X mode obliquely to the magnetic field [16], typically at an angle of the order of 40^{o}, advantage may be taken of the direct cyclotron damping which takes place as the incident wave crosses the cyclotron resonance, that is, before approaching the upper hybrid layer. Due to the increase of X mode damping with $k_{\parallel}$ [7], the plasma optical depth can exceed unity for rays incident in this manner [8] so leading to effective absorption in the thermal electron population. However the antenna requirements are again somewhat inconvenient, and the refractive effect of the plasma is more pronounced at a given level of density for obliquely propagating rays. For normal incidence the cut-off condition may be written as $\beta_e \leq 0.8T_e\%$.

At low toroidal field values typical of small tokamaks it is also practical to consider heating at the second harmonic cyclotron

resonance, the effectiveness of which has also been observed experimentally [4,5]. This has several advantages: firstly, the X mode, which is effectively absorbed, may be launched from an aperture on the low-field side; the theoretical attenuation is fairly insensitive to the value of $k_{\parallel}$; and most of the power is absorbed by electrons with $|v_{\parallel}| \leq v_{the}$. The X mode is reflected when the low density cyclotron cut-off is approached, and as before we can express the limit in terms of electron beta:

$$\beta_e \leq 0.8 T_e \%$$

This is twice as high as the fundamental O mode cut-off value, and the same as that for the fundamental X mode on the high field side, although the required frequency is also doubled for the same value of magnetic field. (In practice however it may be more meaningful to consider the effect of these limits for a given value of source frequency, with resonances obtained by varying the magnetic field. Then it is notable that the density limit is more restrictive at second harmonic resonance, being twice as low as that for the fundamental O mode). Note that although the O mode propagates at densities above the X mode cut-off, its second harmonic damping is very much weaker.

Thus, it would appear that second harmonic resonance heating is quite well suited to low field devices, however several questions arise upon closer theoretical examination. Firstly, as will be shown in the following sections, the plasma may be optically thin or only semi-opaque to the X mode under conditions of interest in small tokamaks. A substantial fraction of the incident radiation is then transmitted across the resonant layer and subsequently reflects off the metallic walls of the torus. Even if the incident beam is

completely polarised in the X mode, the transmitted component is rapidly depolarised in the course of the first few transits of the plasma, by polarisation 'scrambling' at the walls [17] and by polarisation splitting of reflected waves as they enter the plasma. Thus, when the optical depth is low an unpolarised monochromatic radiation field with a broad angular spectrum is rapidly established within the torus, and heating occurs at all points along the vertical extent of the resonant layer. This is somewhat undesirable since the most efficient heating would be expected with localised deposition in the plasma core, and of course power will be lost directly in resistive heating of the walls.

A further question relates to the mechanism through which absorption takes place at second harmonic resonance. Although electrons with parallel velocity in the thermal part of the distribution are responsible for damping the wave, the coupling mechanism becomes stronger as the perpendicular component of electron velocity $v_\perp$ increases: energy is deposited preferentially with electrons of high perpendicular velocity. Furthermore the direct effect of the R.F. heating is to increase the electron kinetic energy of perpendicular motion, so that distortion of the velocity distribution may be induced rather easily as compared with heating at fundamental resonance which increases the perpendicular energy more uniformly with respect to $v_\perp$.

In order to examine in more detail the effect of wall relections we shall consider the linear 2nd harmonic heating that results when the plasma optical depth is low and calculate the radial profile of absorption in a simple model of the toroidal plasma. It will be shown that a geometrical effect leads to a strong local maximum in the heating profile under suitable conditions. This may be simply

understood in terms of the time taken by an electron to cross the resonance layer in the course of its drift motion round a flux surface, and a consideration of electron single particle motion through the resonance leads to a heuristic treatment of the quasi-linear diffusion driven by the waves. From this the critical field strengths are estimated at which collisional relaxation fails to maintain a Maxwellian velocity distribution, and the implications of a quasi-linear 'runaway' are briefly discussed.

2. WAVE PROPAGATION AND ATTENUATION

The two characteristic modes of electromagnetic wave propagation are well described by cold plasma theory except in the vicinity of cut-offs and of the upper hybrid resonance where the phase velocity of the incident X mode drops to a level comparable with the electron thermal speed, thereby leading to a transformation into the electron Bernstein mode. Because the free-space wavelengths of interest are of the order of 1cm or less, the limit of geometrical optics will apply even in small tokamaks, where the inhomogeneity length scale may be of order 10cm. Thus, wave propagation can be discussed in terms of electromagnetic rays which are the trajectories along which the radiant flux of energy takes place. A local wavevector $\underline{k}(r)$ at position $\underline{r}$ is determined along with the trajectory itself by the Hamiltonian ray equations [18] and when dissipation occurs, the power attenuation in a distance s along the ray is conveniently measured by the optical depth τ :

$$\tau = 2\int_0^s \mathrm{Im}k\, \hat{\underline{k}}.d\underline{s}' \qquad (2)$$

where $\hat{k}$ is a unit vector in the direction of the propagation

vector, integration being carried out along the ray. Then disregarding the possible effects of ray focussing, the incident power flux density is attenuated by a factor $e^{-\tau}$. Note that the dissipation is assumed to be weak so that $\mathrm{Im}k \ll \mathrm{Re}k$.

At sufficiently low R.F. power levels, the electron velocity distribution remains Maxwellian in form, and the optical depths may be calculated using the known, linear absorption co-efficients [19]. In general a numerical calculation is necessary for an exact evaluation, however satisfactory estimates may be made using a simple slab model for the cyclotron resonance layer, with the assumption that ray curvature can be neglected. For nearly perpendicular incidence, the resulting expressions are particularly simple, and in the case of the O mode at fundamental resonance one finds [20]

$$\tau_{o1} = \frac{\pi}{2}\left(\frac{kT_e}{mc^2}\right) k_o R_o \frac{\omega_{pe}^2}{\omega^2} n_o \qquad (3)$$

where R_o is the major radius at the centre of the resonance zone, $n_o = \frac{kc}{\omega} = (1-\omega_{pe}^2/\omega^2)^{\frac{1}{2}}$ is the O mode refractive index, and $k_o = \omega/c$. Relativistic corrections are significant when $k_{\parallel} \lesssim k_o\sqrt{kT_e/mc^2}$, but the above non-relativistic result still provides a correct order of magnitude estimate [21]. Clearly the plasma becomes progressively more opaque as the electron temperature, device size and toroidal field become larger, τ_{o1} exceeding unity with $R_o \sim 1\mathrm{m}$ and $B = 2\mathrm{T}$ when $T_e \gtrsim 700\mathrm{eV}$, at electron densities around 50% of the cut-off value, $4 \times 10^{19}\mathrm{m}^{-3}$. On the other hand, electron temperatures in excess of 5keV must be attained before the plasma becomes optically thick in a small device with $R_o \sim 0.3\mathrm{m}$ and $B = 1\mathrm{T}$. Thus, the initial ohmically-heated plasma in small tokamaks will generally be optically thin to the O mode at fundamental resonance.

Similar estimates are possible for second harmonic absorption. Attenuation rates are obtained in the same manner as for fundamental resonance, by expanding the dispersion equation for the electromagnetic wave branches in powers of $\gamma_e = \sqrt{\frac{2kT_e}{m_e c^2}}$. The non-relativistic expression is [19]

$$\kappa_j = \frac{c\,\mathrm{Im}\,k_j}{\omega} = \frac{\sqrt{\pi}}{2} v\,\gamma_e\, n_j^2\, e^{-z_j^2} \frac{\sin^2\theta}{|\cos\theta|} \frac{A_j}{2C+Bn_j^2} \qquad (4)$$

where θ is the angle between the field and the wave-vector; $v = \omega_{pe}^2/\omega^2$, and the indices of refraction n_j for the O(j=1) and X(j=2) modes are given by the Appleton-Hartree formula [15]

$$n_{1,2}^2 = 1 - \frac{2v(1-v)}{2(1-v) - u\sin^2\theta \pm \sqrt{u^2\sin^4\theta + 4u(1-v)^2\cos^2\theta}} \qquad (5)$$

with $u = \Omega_B^2/\omega^2$ taking the value $\frac{1}{4}$.

The variables $z_j = (\omega - 2|\Omega_B|)/n_j\omega\gamma_e\cos\theta$ measure proximity to the resonance centre, and we have defined[1]

$$A_j = n_j^4 \sin^2\theta - n_j^2(1+\cos^2\theta)(1-v) + 2(1-\tfrac{2}{3}v)(1-v-n_j^2\sin^2\theta)$$

$$B = -(1-2v)(1-\tfrac{2}{3}v)\sin^2\theta - (1-v)(1-\tfrac{4}{3}v)(1+\cos^2\theta)$$

and

$$C = (1-v)(1-2v)(1-\tfrac{2}{3}v)$$

In effect the strength of the attenuation is determined for each mode by the quantity $\kappa_j|\cos\theta|$ in Eq. (2). The variation

---

[1] In defining A_j account has been taken of a misprint in the result quoted in Ref. [19].

with incidence angle θ of these functions for a fixed value of $z_{\pm}$ is shown in Fig. 1 over a range of density parameter values. Whereas the X mode attenuation is seen to be substantial over a broad distribution of angles and plasma densities, the damping experienced by the O mode is always much weaker. This property will be explained later in terms of the different wave polarisations and is familiar in the low density theory of cyclotron harmonic emission [22].

An optical depth estimate for the more strongly absorbed X mode at near normal incidence yields [23]

$$\tau_{x2} = 2\pi \frac{kT_e}{mc^2} k_o R_o \frac{\omega_{pe}^2}{\omega^2} \frac{(3-2v)^2}{(3-4v)^2} \sqrt{\frac{(1-2v)(3-2v)}{(3-4v)}} \qquad (6)$$

This result displays the same scaling with device size and temperature as was noted for the fundamental O mode absorption, and its variation with plasma density and magnetic field is broadly similar below cut-off, which occurs when $\frac{\omega_{pe}^2}{\omega^2} = \frac{1}{2}$. In large, high field machines the plasma is generally opaque to this mode, however at the lower temperatures typical of small tokamaks $\tau_{x2} < 1$. For example with $R_o = 0.3$m, $B = 0.5$T and $n_e = 3 \times 10^{18} \bar{m}^3$ we find $\tau_{x2} \simeq 0.19$ at $T_e = 250$eV. The required source frequency in this case would be 28GHz.

As discussed in Section 1.2, therefore, it would appear that multiple reflections of transmitted power must play an important role in determining both the overall plasma heating efficiency and the radial profile of deposition. For the liner material normally used, stainless steel, the theoretical power reflectivity of a plain surface is very high, a typical value at 28GHz (1cm wavelength) being 99.7%. However, irregularities in the wall, including the presence of input and diagnostic ports reduce the effective value by a

significant amount. Nonetheless in TM-3, the cavity Q of the vacuum vessel was found to be ~10^4 at 28GHz in the absence of plasma [24], which implies a mean wall reflectivity of about 99%. If we assume that the additional damping results from all radiation incident on ports being lost then the effective reflectivity is reduced by an amount very nearly equal to the ratio of total port area to total wall area where the latter is an effective value obtained after averaging over short length-scale structures smaller than one wavelength. A port area ratio of around 1% is reasonable, and on the above assumption would be consistent with the wall damping rate in TM-3. Provided that wave absorption in one transit of the plasma between reflections is greater on average than the effective rate of absorption in the walls then the heating efficiency can be high.

As discussed in section 1.2, the radiation field inside the vacuum vessel will, under these conditions of weak damping be essentially unpolarised, and reflections will scatter power into many different directions of propagation, thereby energising all the cavity modes of the torus at the source frequency. In order to study the broad radial heating profiles so produced we can take advantage of these facts in describing the electromagnetic field distribution within the plasma.

3. CALCULATION OF HEATING PROFILES

We have seen that the plasma is immersed in a radiation field which is quite insensitive to the detailed source and antenna characteristics. Thus, we shall assume as an approximation that wall reflections, the natural divergence of the source emission, refraction and polarisation - splitting in the plasma all contribute to the production of a completely unpolarised, monochromatic and

non-directional radiation field. Along any ray path into the plasma then, it will be assumed that the radiant intensity [25] at the plasma edge is the same, I_o say. The magnitude of I_o is determined by the input power and by the level of dissipation, that is by the cavity Q when loaded with plasma.

3.1 Local Heating Rate

In order to determine the heating rate at a chosen point $\underset{\sim}{r}$ in the plasma we need to obtain first the radiant intensities $I_j(\hat{s},\underset{\sim}{r})$ for all directions $\hat{s}$, and modes j, of propagation. These satisfy the equation of radiation transport [25]

$$n_r^2 \frac{d}{ds}\left(\frac{I(\hat{s},\underset{\sim}{r})}{n_r^2}\right) = -\alpha(\hat{s},\underset{\sim}{r})\, I(\hat{s},\underset{\sim}{r}) \qquad (7)$$

where mode subscript j has been omitted, and s denotes arc-length along the ray with direction $\hat{s}$ at $\underset{\sim}{r}$.

The absorption co-efficient α_j is given for the j^{th} mode by $\alpha_j = 2k_o \kappa_j \cos\psi_j$, where κ_j is the damping rate determined for 2nd harmonic absorption by Eq. (4) and ψ_j denotes the angle between the wave vector and group velocity which gives the ray direction $\hat{s}$. Denoting by $d\Omega$ an infinitesimal solid angle about $\hat{s}$, and by $d\Omega_{\underset{\sim}{k}}$ the corresponding solid angle about the wave vector $\underset{\sim}{k}$, the ray refractive index n_r in Eq. (7) is defined by [25]

$$n_r^2 = \frac{n^2}{\cos\psi} \frac{d\Omega_{\underset{\sim}{k}}}{d\Omega} \qquad (8)$$

Integrating Eq. (7) from the point at which the ray enters the plasma at $s = 0$ say, to a point $\underset{\sim}{r}(s)$ at arc-length s, we have

$$I\ (\hat{s},\underline{r}) = n_r^2(\hat{s},\underline{r})\ I_o \exp\left\{ - \int_o^s \alpha(s')ds' \right\}$$

Thus, the local rate at which power is absorbed per unit volume is

$$H(\underline{r}) = \sum_j \int \alpha_j I\ (\underline{r},\hat{s})\ d\Omega = I_o \sum_j \int \alpha_j n_{r_j}^2\ \exp\left\{-\tau(\underline{r},\hat{s})\right\}\ d\Omega \qquad (9)$$

where $\tau(\underline{r},\hat{s})$ is the incomplete optical depth

$$\tau(\underline{r},\hat{s}) = \int_o^s \alpha(s')ds'$$

It is of course implicit that integration is performed only over the range of directions in which a given mode propagates. From the discussion of section 2 we see that typical optical depths are low. As a first approximation we can assume that all rays have low optical depths, although later on we shall allow for the fact that a small proportion of the rays passing through a point in the resonance zone may have exceptionally high optical depth, when $|\hat{s}.\nabla B|$ is small. Setting $\tau \ll 1$ then we have

$$H(\underline{r}) \simeq I_o \sum_j \int \alpha_j n_{r_j}^2\ d\Omega$$

Since $d\Omega_k = \sin\theta d\theta d\phi$ where (θ,ϕ) are the polar angles of $\underline{k}$ about $\underline{B}$, we use Eq. (8) and the definition of α_j to re-express this result in the form

$$H(\underline{r}) = \frac{4\pi I_o \omega}{c} \sum_j \int_o^\pi n_j^2(\underline{r},\theta)\ \kappa_j(\underline{r},\theta)\ \sin\theta\ d\theta \qquad (10)$$

where n_j is the Appleton-Hartree refractive index of Eq. (5), which like κ_j does not depend on azimuthal angle ϕ.

3.2 Surface-Averaged Heating

It can be assumed that the energy absorbed by electrons at a

particular resonance location is distributed rapidly to all parts of the flux surface through this point, on account of the high thermal conductivity along the magnetic field and also by the guiding-centre drift motion of electrons. Thus, it is appropriate to determine the heating rate averaged over the toroidal volume between adjacent flux surfaces:

$$H(\psi) = \oint \frac{H(r)Rd\ell}{|\nabla\psi|} \Bigg/ \oint \frac{Rd\ell}{|\nabla\psi|} \tag{11}$$

where ψ denotes the poloidal flux function, R the major radius, and the line integral is carried out over the flux surface cross-section.

Evaluation of the double integrals in Eq. (11) can be performed numerically, however further simplifications are possible when the maximum resonant layer width ($\theta = 0$) is much less than the major-radial width of the flux surface. Since κ, given by Eq. (4) is expressible in the form $\kappa_j = h_j(\underline{r},\theta)_e^{-z_j^2}$, we can make use of the rapid variation of z with position to approximate Eq. (11) by

$$\oint \frac{Rd\ell}{|\nabla\psi|} H(\psi) = \frac{8\pi I_o \omega}{c} \sum_j \int_o^1 \left[\left\{ n_j^2(\underline{r},\nu) h_j(\underline{r},\nu) \frac{R}{|\nabla\psi|} \right\}_{\underline{r}=\underline{r}_o} \oint e^{-z_j^2} d\ell \right] d\nu \tag{12}$$

where a change of variable to $\nu = \cos\theta$ is made, and we use the symmetry property $n_j(\underline{r},\theta) = n_j(\underline{r},\pi-\theta)$ possessed also by h_j. The minimum value of z_j^2 on the flux surface by definition is attained at $r_o(\psi)$; symmetry of the equilibrium about the mid-plane of the torus is assumed, and with convex surfaces there is a single minimum in the upper half and a corresponding point below. Since $\frac{dz}{d\ell} = -\frac{1}{B}\frac{dB}{d\ell}\left(\frac{1}{n\gamma_e\nu}\right)$ where n (with $u = \frac{1}{4}$) and γ_e are constant on flux surfaces when ν is fixed, a further change of variables yields

$$\oint e^{-z^2} d\ell = 2\int_{z_{min}}^{z_{max}} e^{-z^2} \frac{dz}{\left|\frac{dz}{d\ell}\right|} \doteq 2n\gamma_e \nu \sqrt{\pi} \Big/ \left|\frac{1}{B}\frac{dB}{d\ell}\right|_{\underline{r}=\underline{r}_o} \qquad (13)$$

when resonance is attained at $\underline{r}=\underline{r}_o$, which is assumed to be sufficiently far from the mid-plane that variation of $\frac{1}{B}\frac{dB}{d\ell}$ is negligible in the region where $|z| \lesssim 1$. The limits of integration in z correspond to the two points of greatest distance from resonance and consistent with the above assumption, they are replaced by $\pm\infty$. In general however we must allow for situations where resonance is encountered close to the mid-plane of the torus. To take account of the field variation, which cannot be neglected in these cases, we set $\frac{1}{B}\frac{dB}{d\ell} = g_T(\ell-\ell)^2$ where $g_T = \frac{1}{B}\frac{d^2B}{d\ell^2}_{\ell=\ell_T}$ and T denotes that point of the flux surface which lies closer to resonance, on the mid-plane of the torus. This is satisfactory since the region close to T is most important in determining the integral. The result so obtained may be written as

$$\int e^{-z^2} d\ell = \left|\frac{n\gamma_e \omega\nu}{g_T \Omega_B(\underline{r}_o)}\right|^{\frac{1}{2}} G(z'_T) \qquad (14)$$

where $G(z) = \int_o^\infty y^{-\frac{1}{2}} e^{-(y-z)^2} dy$ and $z'_T = \frac{g_T}{|g_T|} z(\ell_T)$. By redefining z'_T according to

$$z'_T = \frac{g_T}{|g_T|} z(\underline{r}_o) + \frac{|\Omega_B(r_o)|}{n_j \gamma_e \nu\omega |g_T|} \left(\frac{1}{B}\frac{dB}{d\ell}\right)_{\underline{r}=r_o},$$

Eq. (14) is essentially unchanged when the resonance layer lies outside the flux surface ($\underline{r}_o$ coincides with point T) or when $\underline{r}_o$ is close to T. In addition however, when T is well outside the resonance layer centred at $\underline{r}_o$ on the flux surface then $z'_T \gg 1$; and since $G(z) \to \sqrt{\pi/z}$

as $z \to \infty$, Eq. (14) reduces to the form given by Eq. (13). Thus with the modified definition of z_T', all configurations of flux surface and resonance can be described by means of Eq. (14), except that is when the entire flux surface lies inside the resonance zone in which case direct numerical evaluation of Eq. (11) is required. A graph of $G(z)$ is shown in figure 2. The asymptotic form $\sqrt{\pi/z}$ is closely approached for values of $z \geq 4$ and G rapidly approaches zero for $z \leq -2$.

The intensity I_o is determined from a balance between the input power P_s and loss rates in the plasma and wall. The power absorbed by the plasma is

$$P_p = 2\pi \int d\psi H(\psi) \oint \frac{R d\ell}{|\nabla\psi|} ,$$

where the integration extends over the volume of the plasma. Given an effective wall reflectivity ρ the corresponding rate of absorption in the walls is $P_w = 2\pi A_w I_o (1-\rho)$, taking into account that I_o is the incident intensity in each mode. Here A_w is the total wall area and $1 - \rho \ll 1$.

Thus, Eq. (14) determines the profile and strength of the heating when combined with the condition of energy balance $P_s = P_p + P_w$, and the heating efficiency η can be found from $\eta = P_p / P_s$. When resonance is attained under conditions where Eq. (13) is applicable, the heating rate is of an especially simple form, and assuming concentric circular flux surfaces with RB ≃ constant we find

$$H(\psi) \doteq 8\pi k_o I_o \left(\frac{\omega_{pe}^2}{\omega^2}\right)\left(\frac{kT_e}{mc^2}\right) \frac{R}{r \sin \chi_{res}} \sum_j \int_o^1 \frac{(1-\nu^2) n_j {}^5 A_j d\nu}{(2C+Bn_j^2)} \qquad (15)$$

where r is the flux surface radius and χ_{res} denotes the poloidal angle of the resonance point $\underline{r}_o$. From the condition

for validity of Eq. (13), we see that Eq. (15) applies if $|\cos \chi_{res}| < 1 - \frac{n_j R\gamma_e}{r}$. Within this range it is apparent that as the resonance surface approaches tangency with the flux surface the rate of heating becomes locally high as a result of the geometric factor $1/\sin \chi_{res}$. A similar observation has been made by Stix [26] with regard to ion cyclotron resonance heating, and by considering the heating process for single particles this property will be shown in Section 4 to follow directly from the fact that resonance interaction with the wave field is prolonged when a particle drifts vertically through the resonance layer. Equation (15) clearly displays the proportionality of the heating rate to electron temperature and major radius, which is the scaling noted previously of the optical depths (Eq. (6)). Thus the heating profile is broadly distributed over those parts of the plasma accessible to the waves and in contact with the resonance, as expected, but the geometric effect offers the possibility of locally strong heating. Before proceeding to examine this question in detail, however, we shall extend the previous discussion to include the effect of finite optical depth.

3.3 Finite Optical Depth

Although the estimate of Eq. (6) indicates that typical optical depths can be low in cases of interest, there may be particular ray orientations which give rise to exceptionally large path-lengths inside the resonance zone, as for example when a ray propagates vertically at resonance. In such cases ray refraction and toroidal curvature may be the main factors limiting the path length and the resulting optical depths can be markedly higher than average. (Numerical ray-tracing calculations [27] for a small tokamak

configuration indicate that optical depths can be an order of magnitude higher than typical values in a narrow range of such orientations so there may be a significant over-estimate of the associated transmission factors $e^{-\tau}$ in Eq. (10)).

If the optical depth is small when averaged over all ray orientations for any given launching point in the wall, we may still approximate the radiation field by taking I_o to be constant, however it now becomes necessary to write the local heating rate as

$$H(\underline{r}) = 2k_o I_o \sum_j \int n_j^2 (\underline{r}, \theta)\, \kappa_j (\underline{r}, \theta)\, \sin\theta\, d\theta \int_0^{2\pi} e^{-\tau_j(\theta, \phi, \underline{r})}\, d\phi \qquad (16)$$

where ϕ denotes the azimuthal angle of the wave vector about the magnetic field at $\underline{r}$, measured say from the plane in which B does not vary. The incomplete optical depth $\tau_j(\theta, \phi; \underline{r})$, given after Eq. (9), is determined from the ray path through $\underline{r}$ with orientation (θ, ϕ) so that $e^{-\tau_j}$ is the transmission factor with which the energy incident along this ray reaches $\underline{r}$. Using the slab model of the plasma in which only $|B|$ varies, in a direction normal to $\underline{B}$, we can estimate

$$\tau_j(\theta, \phi; \underline{r}) \simeq 2k_o R_o \frac{h_j(\underline{r}, \theta) \cos\psi_j\, \gamma_e |\cos\theta|}{|\sin(\theta + \psi_j)\, \sin\phi|} \left| \int_{\pm\infty}^{z_j(\underline{r},\theta)} e^{-z^2} dz \right| \qquad (17)$$

where the $-\infty$ limit applies when $0 < \phi < \pi$ and $+\infty$ when $\pi < \phi < 2\pi$. Clearly this approximate result breaks down for $\phi \approx 0$ or π : we have neglected ray curvature, and other inhomogeneities, the effects of which are to limit the size of τ_j. Use of Eq. (17) to determine the transmission factors will lead therefore to an underestimate of the heating rate associated with those rays of high optical depth, which should allow comparisons to be made with the results from Eq. (12). Defining

$$\bar{\tau}_{1j}(\underline{r},\theta) = \tau_j(\theta,\pi/2;\underline{r}) \quad \text{and} \quad \bar{\tau}_{2j}(\underline{r},\theta) = \tau_j(\theta,3\pi/2;\underline{r})$$

we find that

$$\int_0^{2\pi} e^{-\tau_j(\theta,\phi;\underline{r})} d\phi = 2\pi\left(T(\bar{\tau}_{1j}) + T(\bar{\tau}_{2j})\right)$$

where

$$T(\mu) = \frac{1}{\pi}\int_1^{\infty} \frac{e^{-\mu x}dx}{x\sqrt{x^2-1}} = \frac{1}{2} - \int_0^{\mu} K_0(y)dy \ ,$$

$K_0(y)$ being the modified Bessel function.

Clearly when $\bar{\tau}_{1j} + \bar{\tau}_{2j} \ll 1$ then we recover the low optical depth result, and in general evaluation of the surface-averaged heating rates from Eq. (11) may be carried out by numerical calculation of the two-dimensional integral over θ and flux-surface arc length ℓ.

3.4 Numerical Calculations

In order to study the detailed profile form we use the above results for the illustrative case of a tokamak with major radius 30cm, plasma minor radius 8cm and toroidal magnetic field in a range of values around 5kG. These parameters are similar to those of TOSCA, and also TM3 (R = 40cm). Only the linear heating problem is considered so the electron temperature is taken to remain fixed with some chosen initial profile. At the chosen value of maximum temperature 300eV, typical optical depths for the X mode are considerably less than unity. The source frequency will be set equal to 28GHz, corresponding to second harmonic resonance at 5kG, so that the more strongly damped X mode will cease to propagate when the density exceeds $0.5 \times 10^{13}\,cm^{-3}$. For simplicity, the flux surfaces are assumed to be circular and concentric, the profiles of density and temperature being parabolic.

In figure 3 the results obtained using Eqs. (12) and (14) are

compared with those obtained firstly by using Eqs. (10) and (11) directly, and secondly by using Eqs. (17) and (16), for the case where resonance occurs at a major radius of 31cm, and the maximum plasma density $3 \times 10^{12}\,cm^{-3}$ is well below X mode cut-off. The level of agreement between the three profiles is surprisingly good, in view of the fact that the resonance half-width is about 1cm and comparable in size therefore with the innermost flux surfaces upon which resonance is attained. The most striking feature of these profiles is the strong local maximum in the heating rate, centred around the flux surface which meets the resonance tangentially, and due to the geometrical effect discussed in Section 3.2. There is a broad distribution of power over surfaces of larger radius all of which cross the resonance, but inside the surface of maximum heating the power drops rapidly with decreasing radius in a characteristic length equal to the resonance layer width, 1cm. For definiteness, we set the effective power reflectivity and radius of the liner equal to 98% and 10cm respectively, (so that the unloaded cavity Q is about 6,000), and normalise the heating rates with respect to an input power of 25kW, which would typically be comparable to the ohmic heating power in TOSCA. Then the radiant intensity $I_o = 8.4$ watts/steradian/cm^2 and the heating efficiency $\eta = 50\%$ giving a mean heating rate of 0.3 watts/cm^3 where the values are taken from the finite optical depth calculation.

As the plasma density approaches the cut-off value, a transition from strongly-peaked to broad, edge-heating profiles takes place as shown in figure 4, (solid lines) obtained for the parameters of figure 3 using the finite optical depth calculation. Associated with the loss of strong heating in the plasma core, there is a drop in heating efficiency and a corresponding rise in the radiant energy

density as measured by I_o. In the case where the electron density reaches 5×10^{12} cm^{-3} at the centre elimination of X mode heating on the flux surface tangential with the resonance allows the small contribution made by the O mode, enhanced by the geometrical effect, to be seen.

At higher values of electron temperature the rate of absorption in the plasma rises, as will the heating efficiency at a given value of plasma density. Setting the peak electron temperature equal to 1200eV, which is near the limit imposed by the condition $\tau_{x2} < 1$ from Eq. (6), we obtain the profile shown (dashed) in figure 3 for density $n_e = 3 \times 10^{13}$ cm^{-3}. Apart from a broadening of the heating maximum consistent with the increase in width of the resonance layer, the profile has a similar character to the 300eV result, although the ratio of peak to average heating rates is now lower.

So far the heating process has been discussed in terms of the wave theory, and in order to specify the damping rates it has been assumed that the electrons have a Maxwellian distribution of velocities. By considering instead the interaction of a single electron with the wave field we can obtain a direct physical understanding of the resonance process and also obtain heuristically the rate co-efficient for velocity space diffusion of electrons driven by the waves. In this way an estimate can be made of the maximum heating rates at which collisions are capable of maintaining a thermal electron distribution.

4. QUASI-LINEAR PROCESSES

4.1 Wave-Particle Interactions

Electrons come into resonance when their drift orbit motion

carries them to a point in the wave where Eq. (1) is satisfied, and in crossing the zone of resonance each experiences a change of velocity which is determined partly by the initial phase of its gyromotion relative to the wave. When phase correlations are destroyed by collisions or other stochastic processes [28] between successive transits of the resonance, then the velocity changes are essentially random and the electrons diffuse in velocity space under the action of the waves.

This leads to a steady increase of the mean electron energy when the distribution of velocities is monotonic and provided that collisions are sufficiently frequent the additional energy is thermalised on the timescale of the heating, the distribution function remaining close to a Maxwellian. Then, apart from a small fraction of magnetically-trapped particles, a typical electron will pass through resonance with nearly constant parallel velocity since we anticipate that the effective interaction time is very much shorter than a typical drift orbit period, and that wave-induced changes in $v_{\parallel}$ will be small. We can neglect the electron guiding-centre drifts and it will be sufficient to represent the electromagnetic field by a superposition of coherent plane waves, provided that the field autocorrelation time is longer than the duration of resonance interaction.

Consider then the perturbing effect of a single plane wave on the motion of an electron about an approximately uniform background magnetic field $\underline{B}_o$. Non-relativistically, we have

$$m \frac{d\underline{v}}{dt} = e\left(\underline{E} + \frac{\underline{v} \times \underline{B}}{c}\right) + e\left(\frac{\underline{v} \times \underline{B}_o}{c}\right) \qquad (18)$$

where $\underline{E}, \underline{B}$ denote the electric and magnetic components of the wave.

Employing Cartesian coordinates (x, y, z), with $\underline{z}$ along $\underline{B}_o$ and y normal to $\underline{k}$, the transverse components of Eq. (18) can be arranged in the form

$$\dot{U}_\pm \pm i\Omega_B(t)\, U_\pm = \frac{e}{m}\{E_\pm + F_\pm\} e^{i(\omega t - k.\underline{r}(t))} \tag{19}$$

where $U_\pm = v_x \pm iv_y$, $E_\pm = E_x \pm iE_y$ and $F_\pm = \frac{1}{\omega}\{(\underline{v}.\underline{E})k_\perp - (\underline{v}.\underline{k})E_\pm\}$, with the oscillatory field variation displayed explicitly. By virtue of slow spatial variations in $|B_o|$, the local gyrofrequency $\Omega_B = \frac{eB_o}{mc}$ at the electron position changes in time, at a rate $\dot{\Omega}_B \simeq v_\parallel \underline{b}.\nabla\Omega_B$ where $\underline{b}$ is a unit vector parallel to $\underline{B}_o$. In the quasi-linear approximation, valid when the resonant change in velocity is small compared to that of the unperturbed motion, we can evaluate the perturbing terms on the right hand side of Eqs. (19) by integrating along the unperturbed trajectory of the electron, viz.

$$z = v_\parallel t \ , \ x = -\frac{v_\perp}{\Omega_B}\cos\psi \ , \ y = \frac{v_\perp}{\Omega_B}\sin\psi$$

where $\psi = \int_{t_o}^{t} \Omega_B(t')dt'$, t_o being an initial instant when the gyrophase is 0. Choosing $e^{\pm i\psi(t)}$ as integrating factor Eq. (19) can thus be solved readily to yield

$$\begin{aligned} e^{\pm i\psi(t)} U_\pm(t) &= U_\pm(t_o) \\ &+ \frac{e}{m}\left[\left\{E_\pm\left(1 - \frac{k_\parallel v_\parallel}{\omega}\right) + \frac{k_\perp v_\parallel}{\omega}E_z\right\}\int_{t_o}^{t} e^{i\left[(\omega - k_\parallel v_\parallel)t' \pm \psi(t') + a\cos\psi(t')\right]}\, dt' \right. \\ &\left. + \frac{k_\perp v_\perp}{\omega}E_y \int_{t_o}^{t} e^{i\left[(\omega - k_\parallel v_\parallel)t' + a\cos\psi(t')\right]}\, dt' \right] \end{aligned} \tag{20}$$

where $a = \frac{k_\perp v_\perp}{\Omega_B}$. Using the expansion $e^{ia\cos\psi} = \sum_{m=-\infty}^{\infty} J_m(a)\, e^{im(\frac{\pi}{2} - \psi)}$

each of the integrals in Eq. (20) can be replaced by a sum of terms of the form $\sum_{m=-\infty}^{\infty} J_{m+r}(a) e^{i(m+r)\frac{\pi}{2}} \int_{t_o}^{t} \exp i\left[(\omega - k_{\parallel}v_{\parallel})t' - m\psi(t')\right] dt'$ where $r = \pm 1$ for the first integral, and $r = 0$ for the second. If the electron encounters n^{th} harmonic resonance in the course of its motion at time $t = t_{res}$, say, so that $\omega - k_{\parallel}v_{\parallel} = -n\Omega_B(t_{res})$ (taking account of the negative sign of Ω_B), then an integrand in the above sum of terms will vary slowly for $t' \approx t_{res}$ if $m = -n$. For all other values of m however the integrands oscillate rapidly so that for $(t - t_o)|\Omega_B(t_{res})| \gg 1$ they give rise to negligibly small contributions in the summation. Since the dominant contribution to the $m = n$ integral arises from values of t' close to t_{res} we expand $\psi(t')$ in Taylor series about the resonance point and obtain

$$\int_{t_o}^{t} \exp i\left[(\omega - k_{\parallel}v_{\parallel})t' + n\psi(t')\right] dt' \simeq$$

$$e^{in\left[\psi(t_{res}) - \Omega_B(t_{res})t_{res}\right]} \int_{t_o}^{t} \exp i\left[\frac{n\dot{\Omega}_B(t_{res})}{2}(t' - t_{res})\right] dt'$$

In the limits $(t_{res} - t_o)$, $(t - t_{res}) \gg \left\{2/n|\dot{\Omega}_B|\right\}^{\frac{1}{2}}$ the above integral is easily evaluated and so Eq. (20) then yields

$$e^{\pm i\psi(t)}U_{\pm}(t) = U_{\pm}(t_o) + \frac{e}{m}\left[\left\{E_{\pm}\left(1 - \frac{k_{\parallel}v_{\parallel}}{\omega}\right) + \frac{k_{\perp}v_{\parallel}}{\omega}E_z\right\} J_{n\pm1}(a) \pm iE_y\left(\frac{k_{\perp}v_{\perp}}{\omega}\right)J_n(a)\right] \sqrt{\frac{2\pi i}{n|\dot{\Omega}_B|}}\, e^{i(\Xi \pm \frac{\pi}{2})} \qquad (21)$$

where $\Xi = n(\psi(t_{res}) - \Omega_B(t_{res})t_{res}) + (\frac{n+2}{2})\pi$. The first term represents the unperturbed gyromotion and the second gives the resonant change in transverse velocity $v_\perp$, which we can see is produced in a characteristic time $\Delta t_{res} = \sqrt{\frac{2\pi}{n|\dot{\Omega}_B|}}$ where $\dot{\Omega}_B$ is evaluated at the point of resonance. As we shall see later Δt_{res} is generally much shorter than the electron drift orbit period. From Eq. (21) we obtain $v_x = \frac{1}{2}\mathrm{Re}(U_+ + U_-)$ and $v_y = \frac{1}{2}\mathrm{Im}(U_+ - U_-)$, and so determine the resonant change of transverse kinetic energy $\frac{1}{2}mv_\perp^2$. This may be expressed in terms of the complex quantity

$$\Delta v = \frac{e}{m}\mathcal{E}\Delta t_{res} \tag{22}$$

where $\mathcal{E}$ is an effective electric field given by

$$\mathcal{E} = \left\{E_x \frac{nJ_n(a)}{a} + iE_y J_n'(a) - \frac{v_\parallel}{v_\perp} E_z J_n(a)\right\}\left(\frac{\omega - k_\parallel v_\parallel}{\omega}\right) e^{i\Xi} \tag{23}$$

The magnitude of the perpendicular velocity after resonance is then given by

$$v_\perp^2 = v_{\perp o}^2 + 2|\Delta v_\perp|\cos\Xi + |\Delta v_\perp|^2$$

where $v_{\perp o}$ denotes the initial value of $v_\perp$. Clearly, the value of the increment depends through Ξ on the initial gyrophase of the electron relative to the wave. Stochastic heating calculations for mirror machine geometry based on an analysis similar to this were carried out by Lieberman and Lichtenberg [28].

By integrating the component of Eq. (18) parallel to $\underline{B}_o$, making use of the above methods we obtain the resonant change in $v_\parallel$:

$$\Delta v_{\parallel} = \mathrm{Re}\left\{\frac{k_{\parallel} v_{\perp}}{\omega - k_{\parallel} v_{\parallel}} \frac{e}{m} \mathcal{E} \Delta t_{res}\right\} \tag{24}$$

Since $kc/\omega \sim O(1)$ for electromagnetic waves we see that $\Delta v_{\parallel} \sim \frac{v}{c} |\Delta v_{\perp}|$ so that the dominant effect is the change of perpendicular velocity during resonance. (In the case of Bernstein waves however, $k \sim \omega v_{the}$ so that $v_{\parallel}$ and $v_{\perp}$ can change by similar amounts).

For tokamak geometry, we have $\dot{\Omega}_B \sim O\left(\frac{r}{R} \frac{v_{\parallel} \Omega_B}{R}\right)$ and since the drift orbit period of an electron $\tau_{tr} \sim O\left(\frac{R}{v_{\parallel}}\right)$, then $|\Omega_B \Delta t_{res}| \sim \frac{\tau_{tr}}{\Delta t_{res}} \sim \sqrt{\frac{R}{r} \frac{R|\Omega_B|}{v_{\parallel}}} \gg 1$, so that although the electron performs many Larmor gyrations during resonance, the zone of interaction is well localised on the drift orbit.

In addition, for a typical gyrotron bandwidth of 0.1% at 30GHz the auto-correlation time is of order $3\text{-}4 \times 10^{-8}$ sec which is significantly longer in general than Δt_{res} for the parameters of section 3.4. This justifies our use of a coherent wave representation of the R.F. field.

4.2 Velocity Space Diffusion

Assuming as discussed earlier that electron-wave phase correlations are destroyed in a time less than the orbit period τ_{tr}, the phase angle Ξ will change randomly as the electron performs successive transits and the perpendicular velocity will undergo a random walk with step size $|\Delta v_{\perp}|$ and frequency τ_{tr}^{-1}. The heating process is thus characterised by a velocity diffusion co-efficient

$$D_{\perp} = \frac{1}{2} \left\langle \Delta v_{\perp}^2 \right\rangle \tau_{tr}^{-1} \tag{25}$$

where $\left\langle \Delta v_{\perp}^2 \right\rangle = \frac{1}{2} |\Delta v_{\perp}|^2$ is the mean square step-size, and the flux-

surface averaged electron distribution function f satisfies a diffusion equation of the form

$$\frac{\partial f}{\partial t}=\frac{1}{v_\perp}\frac{\partial}{\partial v_\perp}\left(v_\perp D_\perp \frac{\partial f}{\partial v_\perp}\right) + C_e(f)$$

where $C_e(f)$ represents the electron collision terms. The drift period for circulating electrons is $\tau_{tr} \simeq \frac{2\pi qR}{v_\parallel}$ where q is the safety factor, and $\dot{\Omega}_B \simeq \frac{v_\parallel \Omega_B}{qR}\frac{r}{R}\sin\chi_{res}$. In the limit of small Larmor radius $|a| \ll 1$ therefore, Eq. (25) yields

$$D_\perp = \frac{1}{2^{2(n+1)}\{(n-1)!\}^2}\left(\frac{e}{m}\right)^2 \left|E_x + iE_y + \frac{k_\parallel v_\parallel}{\omega}E_z\right|^2 \left(\frac{k_\perp v_\perp}{\Omega_B}\right)^{2(n-1)} \frac{R}{r\omega \sin\chi_{res}} \qquad (26)$$

Note that the electron crosses resonance twice per orbit: Eq. (26) gives the diffusion rate due to each interaction zone separately. This heuristically derived expression may be compared with the result obtained more formally by Rowlands et al [29] from the quasi-linear theory for spatially homogeneous systems. Taking account of a change in sign convention for the wave vector, Eq. (26) is seen to be of the same form as the wave diffusion co-efficient in a homogeneous plasma, the main difference being that the effective interaction time in a uniform magnetic field is determined by the rate at which an electron crosses a wave packet.

Several characteristic properties of cyclotron harmonic absorption are evident from Eq. (26). Firstly we see that as one would expect, the coupling to electrons occurs primarily through the right-hand circularly polarised component of the field (E_x+iE_y),

which rotates in the direction of electron gyromotion. Thus, the strong right-handed component of the X mode at frequencies $\omega > |\Omega_B|$ gives rise to higher damping rates at the cyclotron harmonics than does the O mode which has a much weaker component in this polarisation. At very low densities such that $\omega_{pe}^2 \lesssim \omega^2 \frac{kT_e}{mc^2}$ this is true also at the fundamental resonance, however in cases of interest where $\omega_p^2/\omega^2 \sim O(1)$, the dielectric response of the plasma strongly modifies the wave polarisations when $\omega \simeq |\Omega_B|$ such that for general angles of propagation, $\frac{E_x+iE_y}{|E|} = O\left(\frac{(\omega-|\Omega_B|)}{\omega_p^2}\omega\right)$, for both modes. A more detailed examination of the wave polarisation shows that the O mode coupling is strongest for $\underline{k}.\underline{B} = 0$, whereas that for the X mode is strongest at parallel propagation, as can be seen also from the linear wave attenuation rates given by Litvak et al. [7].

A second important property manifest in Eq. (26) is a power dependence of the diffusion rate on the electron perpendicular velocity for harmonic resonance, alluded to in section 1.2. For the higher harmonics especially, therefore, the wave-driven diffusion will tend to distort the perpendicular velocity distribution from a Maxwellian. This in turn will affect the rate of absorption in the plasma, even though the parallel velocity distribution, by Eq. (24), is only weakly altered. By contrast, the diffusion rates for fundamental heating, given by Eq. (26) depend only on $v_\parallel$, so we expect the linear heating rate to be much less sensitive to changes in the perpendicular velocity distribution induced by the heating. This is confirmed by explicit solution of the diffusion equation [29].

A final observation from Eq. (26) is to note the dependence of the coupling strength on the geometrical factor $\frac{R}{r \sin \chi_{res}}$, previously found in the linear heating rate given by Eq. (15). This can now be

interpreted as an effect due to a reduction of the rate at which the Larmor frequency changes along the electron trajectory through resonance when $\sin\chi_{res}$ is small. In fact, using Eqs. (22) and (23), the flux-surface-averaged heating rate can be calculated following a method similar to that used by Stix [26] for ion cyclotron heating. This gives

$$P = \frac{1}{2^{2n+1}\{(n-1)!\}^2} \frac{e^2 R}{mr|\Omega_B|\sin\chi_{res}} \int \left| E_x + iE_y + \frac{k_\perp v_\parallel}{\omega} E_z \right|^2 \left(\frac{k_\perp v_\perp}{\Omega_B}\right)^{2(n-1)} f_e(\underline{v}) d^3\underline{v} \tag{27}$$

where f_e is the electron velocity distribution function, and where we allow for the fact that each electron crosses resonance twice per orbit, symmetry about the mid-plane being assumed. Comparing Eqs. (15) and (27) for the second harmonic absorption, we see that T_e in the former is to be interpreted as the mean perpendicular energy. At the fundamental, since $E_x + iE_y \sim 0\left(\frac{k_\parallel v_\parallel}{\omega_p^2}\omega\right)$, Eq. (27) shows that the heating rate is determined by the parallel velocity distribution, which as we noted before is only weakly influenced by the direct effects of the waves.

4.3 Threshold Estimates for Quasi-Linear Diffusion

Neglecting the effects of toroidal geometry on electron drift motion, valid for the majority of circulating particles, we can estimate the heating rate beyond which quasi-linear distortion of the velocity distribution becomes strong, by obtaining a condition for balance within the thermal electron population between the rate of diffusion due to the waves and the rate at which Coulomb collisions restore thermal equilibrium.

By inspecting Eq. (27) it is seen that electrons with $v_{Te} \lesssim v_\perp \lesssim 2v_{Te}$ are most important in determining the second

harmonic heating when f_e is Maxwellian. Also since the diffusion rate given by Eq. (27) depends only weakly on $v_{\parallel}$, pitch-angle scattering is less important than collisional slowing down, so a threshold intensity may be obtained from the condition that $D_{\perp}(v_{\perp}) \lesssim \frac{1}{2} v_{\perp}^2 \nu_s$, for all $v_{\perp} < 2v_{Te}$ where ν_s is the rate at which an electron of velocity $v \sim v_{\perp}$ slows down and $D_{\perp}$ is the appropriate quasi-linear diffusion coefficient.

In order to employ this argument in relation to the second harmonic heating discussed in Section 3, where the wave spectrum is broad, we assume that the electron interacts with each spectral component independently so that the total diffusion co-efficient may be formed by integrating Eq. (25) over $k_{\parallel}$. This is justified since the interaction time Δt_{res} with any component is much less than the time during which the electron is in resonance with the wave spectrum as a whole, and also since no phase correlations will exist between different components. Then the total rate of diffusion, allowing for resonance above and below the mid-plane, is

$$D_{\perp} = \frac{\pi}{4} \left(\frac{e}{m}\right)^2 \int P \frac{W}{(n^2+N)} \left(\frac{kv_{\perp}}{\Omega_B}\right)^2 \sin^2\theta \left(\frac{R_o}{r\omega \sin \chi_{res}}\right) d\Omega_k \qquad (28)$$

where $P(\theta, r, \chi_{res}) = \left| E_x + iE_y + \frac{k_{\perp} v_{\parallel}}{\omega} E_z \right|^2 \Big/ |E|^2$, and $W = \frac{1}{8\pi} |E|^2 (n^2+N)$ denotes the spectral energy density of the wave field such that $W d\Omega_K$ is the field energy per unit volume associated with the solid angle of wave vector directions $d\Omega_k$ about $\underline{k}$. The quantity $N = \underline{E}^* . \frac{\partial}{\partial \omega} (\omega \underline{\underline{\varepsilon}}) . \underline{E} / |E|^2$ determines the electric field and kinetic energy densities. Note that χ_{res} varies with $k_{\parallel}$.

In terms of the radiant intensity I, W is given by $W = \frac{kI}{|\underline{k} . \underline{v}_G|} \frac{n^2}{n_r^2}$ where the ray refractive index n_r is given by Eq. (8), and $\underline{v}_G$ denotes the group velocity. Well below cut-off, $n \sim n_r \sim N \sim 1$ and

$\underline{v}_G \simeq c\hat{\underline{k}}$ so $W \sim I/c$. Also $P \sim O(1)$ for the X mode so the threshold criterion for thermal electrons reduces to the approximate form

$$\frac{4\pi^2}{3} \frac{|\Omega_B|}{\nu_s} \frac{I}{c_B^2} \frac{R_o}{r \sin \chi_{res}} \lesssim 1 \qquad (29)$$

when the variation of χ_{res} with $k_{\parallel}$ can be neglected. With ν_s determined by electron-ion and electron-electron friction, $\nu_s \simeq 3 \times 10^{-8} n_e \left(\frac{300}{\frac{1}{2} mv^2}\right)^{3/2}$ $^{-1}$ sec, for $v > v_{Te}$, where n_e is in cgs units and mv^2 is in eV, so for the parameters of Section 3.4, condition (29) yields

$$I < 190 \left(\frac{n_e}{10^{12}}\right)\left(\frac{T_e}{300}\right)^{-3/2} \frac{r}{a} \sin \chi_{res} \text{ watts/cm}^2\text{/steradian}$$

Applied to the case represented in figure 3, the above condition yields an upper limit of about 200 watts/cm^2/steradian for the flux surface of radius 3cm ($\chi_{res} \simeq 70^o$), so that the criterion for a thermal electron distribution there is well satisfied at an input power of 25kW, since $I_o \sim 10$ watts/cm^2/steradian. Clearly condition (29) becomes more stringent as the flux surface tangential with resonance is approached, and when $\chi_{res} \simeq 0$ or π then Eq. (28) is no longer valid, since the variation of $\frac{d\Omega_B}{dt}$ during resonance cannot be neglected. There is therefore a minimum value of χ_{res} (or $\pi - \chi_{res}$) below which the diffusion rate, no longer given by Eq. (26), reaches a maximum value and then falls rapidly when the flux surface no longer crosses resonance. This minimum angle is attained when an electron drifts from the point of resonance to the midplane of the torus in a time comparable with the interaction time Δt_{res} . Then Eq. (29) is seen to apply when $\sin \chi_{res} \gtrsim \left|\frac{2\pi v_{\parallel}}{rq\omega}\right|^{1/3}$,

which leads to a maximum value of the resonance time $\Delta t_{res} \simeq \left\{\frac{2\pi}{\omega}\left(\frac{Rq}{v_{\parallel}}\right)^2 \frac{R}{r}\right\}^{1/3}$. Replacing $\sin\chi_{res}$ in Eq. (25) by this lower limit gives a stronger threshold condition for electrons on surfaces where resonance with all parts of the spectrum is encountered close to the midplane of the torus. With parameters used above we then find

$$I < 30 \left(\frac{n_e}{10^{12}}\right)\left(\frac{300}{T_e}\right)^{4/3}\left(\frac{r}{a}\right)^{2/3} \text{ watts/cm}^2\text{/steradian} \qquad (30)$$

where the safety factor $q \sim 1$.

For the surface of maximum heating in figure 3, $r \simeq 1$cm and this yields $I < 23$ watts/cm^2/steradian, so the condition for linear heating at all radii in the initial 300eV plasma is satisfied in the case discussed for input power levels lower than about 70kW, given the assumed wall absorption rate of 2%.

When the electron density is higher so that the central parts of the plasma are inaccessible to the X mode, we have seen from figure 4 that a broad distribution of power over the outer surfaces in contact with resonance takes place, those surfaces where χ_{res} is small being cut off. Condition (29) is then sufficient to estimate the threshold intensity on the surface of maximum heating where the density is well below cut off. Thus, for the case in figure 4 where $n_e = 5 \times 10^{12}$ cm^{-3}, maximum heating occurs around the surface $r = 4$cm, and condition (26) yields a threshold of about 500 watts/cm^2/steradian, which greatly exceeds those of the previous example because of the much lower heating rate per electron.

As the temperature rises under the influence of the R.F. power, or when the input power in increased, the linear threshold is normally exceeded first on the surface of maximum heating and when this occurs

electrons in the local thermal population will start to 'run away' to high values of perpendicular energy, in the absence of any mechanism of relaxation other than collisions. Not only will these electrons become decoupled from the remainder of the thermal population, but they will also absorb the incident R.F. power with greater efficiency as their Larmor radii expand [30]. This is clearly undesirable as the effective bulk plasma heating rate will be significantly reduced. A similar runaway of superthermal electrons can take place below threshold but is less serious in this case because a much smaller proportion of electrons is involved. A further consequence of perpendicular runaway is that due to the toroidal geometry, electrons will become trapped in banana orbits as they are heated when $v_\perp \gg v_\parallel$ and eventually will turn in the resonance region, as in applications of ECRH to mirror machines [31]. The trapping of a significant fraction of electrons in this way could modify the plasma current density profile and possibly lead to other deleterious effects on confinement. Note that such effects of trapping would also be evident in fundamental heating, when $D_\perp \gtrsim \frac{1}{2} v_{Te}^2 \nu_s$.

5. CONCLUSIONS

High-frequency plasma heating, using the second electron cyclotron harmonic resonance, in small, low-field tokamaks such as TOSCA has been discussed, and linear heating profiles calculated for cases of interest where the plasma is optically thin, so that wall reflections are important. It is shown that maximum heating at smaller minor radii is favoured by a geometrical effect of the flux-surface and resonance configuration. A simple, heuristic argument leads to expressions for the quasi-linear rates of electron diffusion in velocity space, providing a clear physical picture of the heating process and indicating several important general properties. In particular, second harmonic electron

heating rates are seen to increase with kinetic energy transverse to the magnetic field. If the R.F. heating fields are sufficiently intense then thermal electrons will be driven to high transverse velocity, resulting in an increase of the trapped electron population with possibly damaging consequences for confinement and stability. A threshold criterion is given for heating rates below which this may be avoided, and used to estimate maximum input power levels. These indicate that heating rates well above that supplied typically by Ohmic dissipation should be possible.

Acknowledgements

The author is indebted to Drs C.N. Lashmore-Davies, W.H.M. Clark, A.C. Riviere and D.C. Robinson of Culham Laboratory for helpful discussions on many aspects of this work, and also to Dr R. Cano of C.E.N. Fontenay-aux-Roses for an illuminating discussion on second harmonic absorption.

REFERENCES

[1] LICHTENBERG A.J., SCHWARTZ M.J., TUMA D.T., Plasma Physics 11 (1969) 101.

[2] RIVIERE A.C., ALCOCK M.W. and TODD T.N., Proc. 3rd Topical Conf. on Radio Frequency Plasma Heating, Pasadena (1978) Vol. II, p. 3.

[3] ALIKAEV V.V. et al., Proc. Joint Varenna-Grenoble Int. Symposium on Heating in Toroidal Plasmas (1978) Vol. II, p. 339. See also the paper by H.R. Jory, ibid, p. 351.

[4] ALIKAEV V.V. et al. Sov. Jnl. Plasma Physics 2 (1976) 212.

[5] STRELKOV V.S. Proc. 9th. European Conf. on Controlled Fusion and Plasma Physics, Oxford (1979).

[6] TRUBNIKOV B.A. in Plasma Physics and the Problem of Controlled Thermonuclear Reactions, ed. M.A. Leontovich, vol. III, p. 122, Pergamon Press, New York (1959).

[7] LITVAK A.G. et al., Nuclear Fusion 17 (1977) 659.

[8] ALIKAEV V.V. et al., Sov. Jnl. Plasma Physics 3 (1977) 127.

[9] FIDONE I. et al., Phys. Fluids 21 (1978) 645.

[10] EFTHIMION P.C. et al. Phys. Rev. Letters 44 (1980) 396.

[11] McGUIRE K., ROBINSON D.C., WOOTTON A.J., Proc. 7th Int. Conf. on Plasma Physics and Controlled Thermonuclear Fusion, Innsbruck, IAEA-CN-37/T1-1 (1978).

[12] MAROLI C. and BORNATICI M., Proc. Varenna Workshop on Plasma Transport, Heating and MHD Theory, p. 243 CEC (1978)

[13] STIX T.H., Phys. Rev. Letters 15 (1965) 878.

[14] KOCHETKOV V.M., Sov. Phys. Tech. Phys. 21 (1976) 280.

[15] GINSBURG V.L., The Propagation of Electromagnetic Waves in Plasmas, Pergamon Press, Oxford (1964).

[16] GILGENBACH R.M. et. al., Phys. Rev. Letters 44 (1980) 647.

[17] COSTLEY A.E. et. al., Phys. Rev. Letters 33 (1974) 758.

[18] BERNSTEIN I., Phys. Fluids 18 (1975) 320.

[19] AKHIEZER A.I. et. al., Plasma Electrodynamics, Vol.I., Pergamon Press, Oxford (1975).

[20] LITVAK A.G. et. al., Sov. Tech. Phys. Letters 1 (1975) 374.

[21] BORNATICI M. and ENGELMANN F., Radio Science 14 (1979) 309.

[22] ENGELMANN F. and CURATOLO M., Nuclear Fusion 13 (1973) 497.

[23] MANHEIMER W.M., 'Electron Cyclotron Heating in Tokamaks' in Infra-Red and Millimeter Waves, Vol. II, ed K.J. Button Academic Press, New York (1979).

[24] ALIKAEV V.V. et. al., JETP Letters, 15 (1972) 27.

[25] BEKEFI G., Radiation Processes in Plasmas, John Wiley, New York (1966).

[26] STIX T.H., Nuclear Fusion 15 (1975) 737.

[27] FIELDING P.J., Unpublished.

[28] LIEBERMAN M.A. and LICHTENBERG A.J., Plasma Physics 15 (1973) 125.

[29] ROWLANDS G., SIZONENKO V.L. and STEPANOV K.N., Sov. Phys. JETP 23 (1966) 661.

[30] FIDONE I., GRANATA G. and MEYER R.L., Report EUR-CEA-FC1017 (1979).

[31] JAEGER F., LICHTENBERG A.J. and LIEBERMAN M.A., Plasma Physics 14 (1972) 1073.

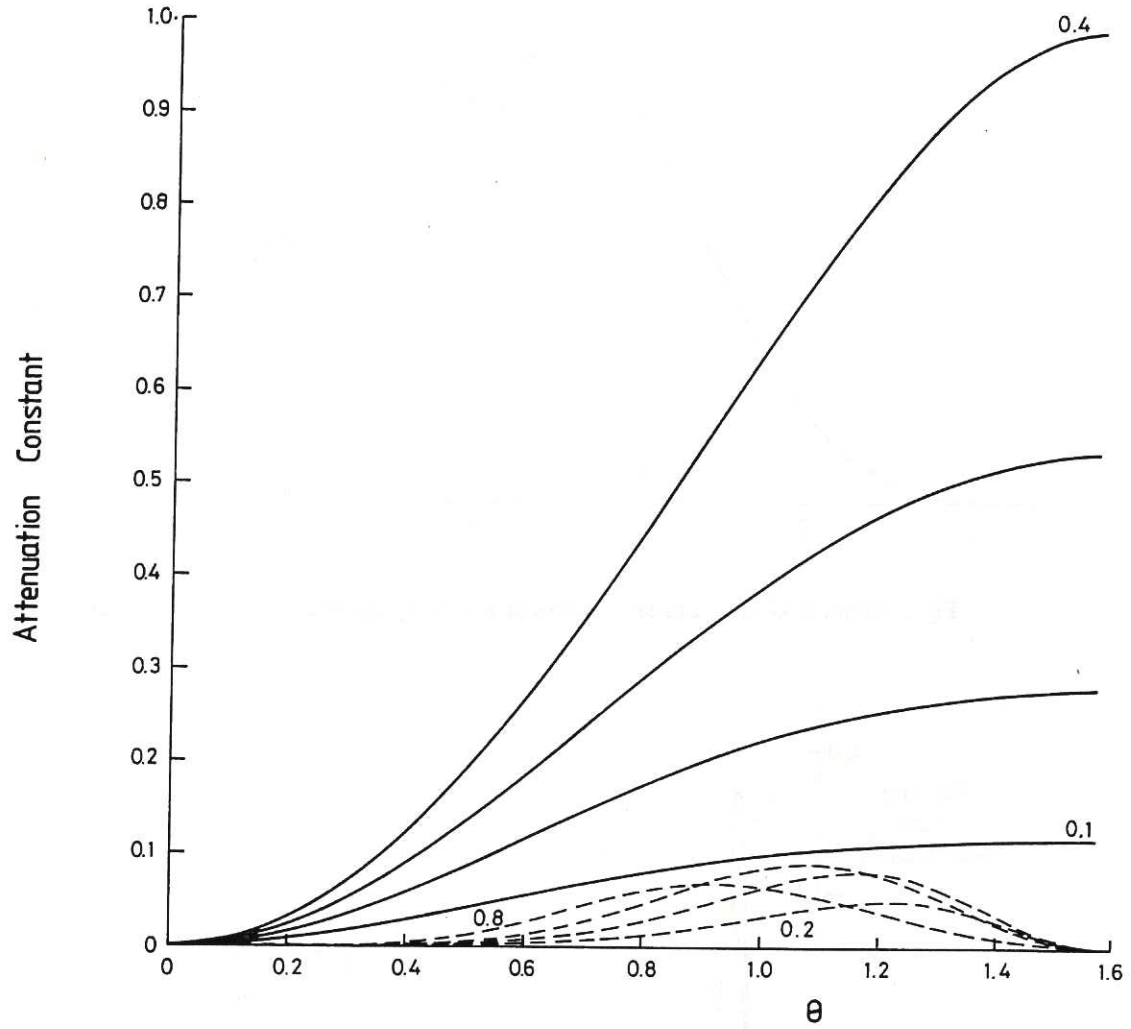

Fig.1 Variation of the second harmonic attenuation constants with angle of incidence, over a range of values of $v = \frac{\omega_{pe}^2}{\omega^2}$, for the extra-ordinary mode (solid lines, v = 0·1, (0·1), 0·4) and the ordinary mode (dashed lines, v = 0·2, (0·2), 0·8). The 0 mode curves are magnified ten times relative to those for the X mode, for greater clarity.

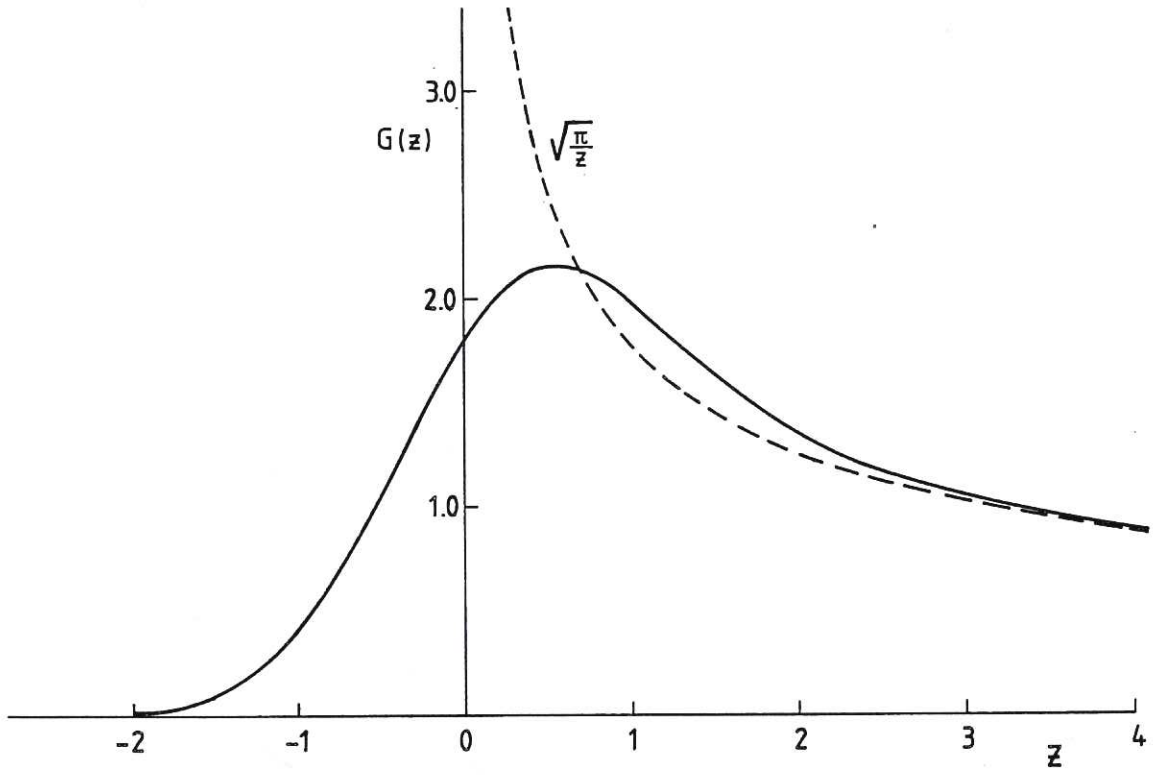

Fig.2 Graph of G vs z. For large values of z, G is asymptotic to $\sqrt{\pi/z}$ (dashed).

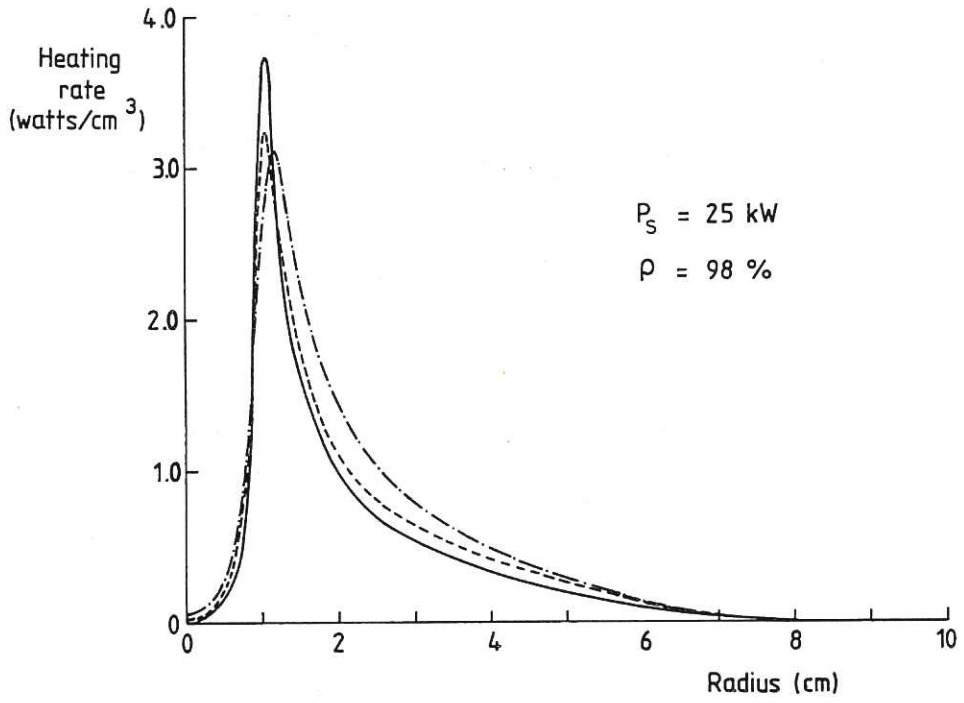

Fig.3 A comparison of the radial heating profiles obtained for the same case, using (a) Eq.(10) (——), (b) Eq.(12) (-·—·—) and (c) Eqs.(16) and (17) (----). The density and temperature profiles are taken to be parabolic, and on axis $n_e = 3 \times 10^{12}/cm^3$, $T_e = 300$ eV and $B_\phi = 5{\cdot}17$ kG. Source frequency 28 GHz.

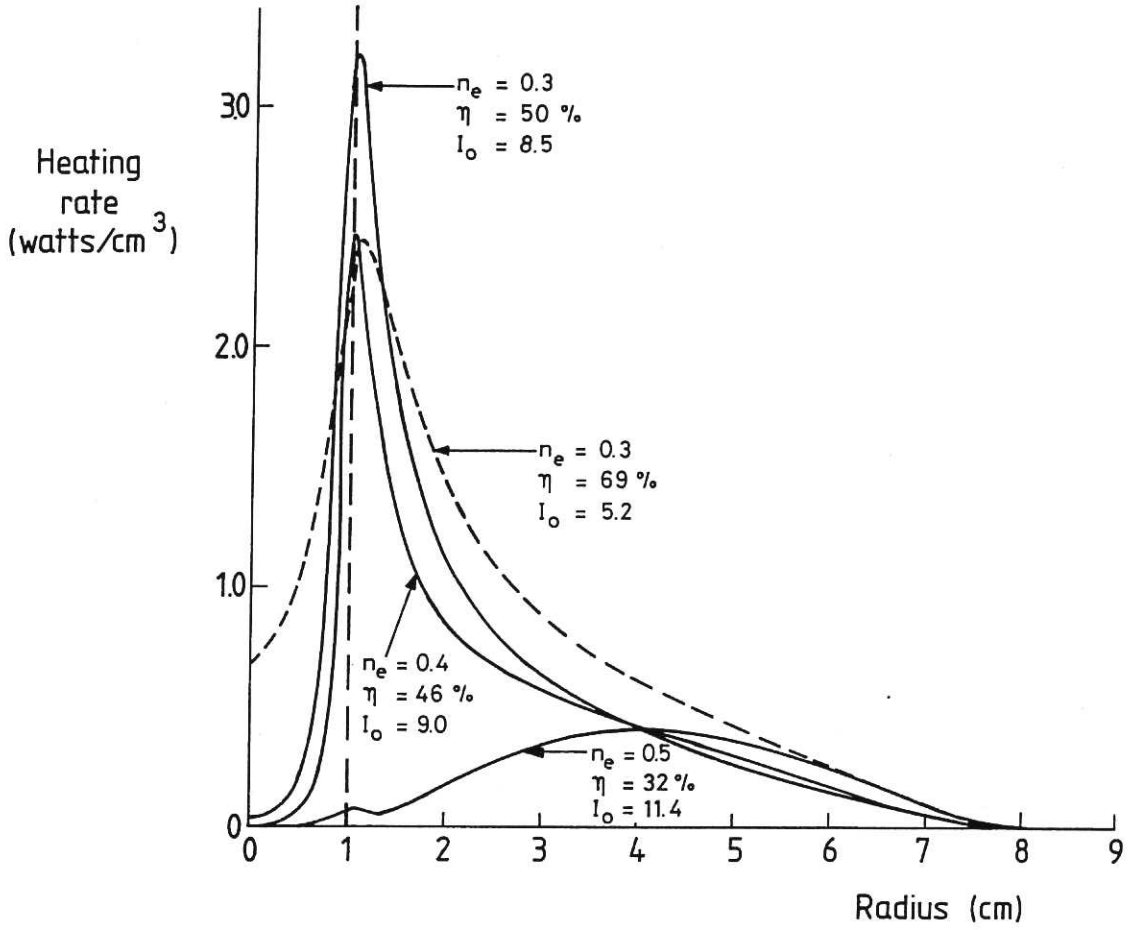

Fig.4 Variation of the heating profile with increasing plasma density n_e (in units of $10^{13}/cm^3$). As the X mode cut-off density (n_e = 0·5) is approached a rapid transition to edge heating occurs, the absorption efficiency η falls, and the radiant intensity I_0 (in watts/cm^2/ster.) within the torus rises.